

## Activation priming and cytokine polyfunctionality modulate the enhanced functionality of low-affinity CD19 CAR T cells

Tracking no: ADV-2022-008490R1

Ilaria Michelozzi (UCL Great Ormond Street Institute of Child Health, United Kingdom) Eduardo Gomez-Castaneda (UCL Great Ormond Street Institute of Child Health, United Kingdom) Ruben Pohle (UCL Great Ormond Street Institute of Child Health, United Kingdom) Ferran Cardoso Rodriguez (Cell Communication Lab, Department of Oncology, University College London Cancer Institute, United Kingdom) Jahangir Sufi (Cell Communication Lab, Department of Oncology, University College London Cancer Institute, United Kingdom) Pau Puigdevall-Costa (Genetics and Genomic Medicine Department, Great Ormond Street Institute of Child Health, United Kingdom) Meera Subramaniam (UCL Great Ormond Street Institute of Child Health, United Kingdom) Efstratios Kirtsios (UCL Great Ormond Street Institute of Child Health, United Kingdom) Ayad Eddaoudi (University College London, ) Si Wei Wu (Terry Fox Laboratory, Canada) Aleks Guvenel (UCL Great Ormond Street Institute of Child Health, United Kingdom) Jonathan Fisher (Developmental Biology and Cancer Section, UCL Great Ormond Street Institute of Child Health, United Kingdom) Sara Ghorashian (Great Ormond Street Hospital for Children NHS Foundation Trust, United Kingdom) Martin Pule (University College London, United Kingdom) Christopher Tape (Cell Communication Lab, Department of Oncology, University College London Cancer Institute, United Kingdom) Sergi Castellano (Genetics and Genomic Medicine Department, Great Ormond Street Institute of Child Health, United Kingdom) Persis Amrolia (Great Ormond St Children's Hospital, United Kingdom) Alice Giustacchini (UCL Great Ormond Street Institute of Child Health, United Kingdom)

### Abstract:

changes occurring in T-cells expressing low-affinity vs high-affinity CD19 CARs following stimulation with CD19-expressing cells. Our results show that CAT CAR T-cells exhibit enhanced activation to CD19 stimulation and a distinct transcriptomic and protein profile, with increased activation and cytokine polyfunctionality compared to FMC63 CAR T-cells. We demonstrate that the enhanced functionality of low-affinity CAT CAR T-cells is a consequence of an antigen-dependent priming induced by residual CD19-expressing B-cells present in the manufacture.

**Conflict of interest:** No COI declared

**COI notes:**

**Preprint server:** Yes; biorxiv 10.1101/2020.09.22.291831

**Author contributions and disclosures:** I.M.M. designed, performed and analyzed experiments, performed bioinformatic analyses of mass cytometry experiments and contributed to writing the manuscript. E.G-C performed bioinformatic analyses of transcriptomic data and wrote the relative bioinformatic supplementary information. R.V.C.P. performed experiments and bioinformatic analyses of mass cytometry and transcriptomic data. F.C-R provided data analysis tools and contributed to bioinformatic analyses of mass cytometry experiments. P.P-C. performed transcriptomic bioinformatic analyses data checks and contributed to writing the bioinformatic supplementary information. J. S., M.S., S.W.W, A.Gu. and E.K. performed experiments. A.E. provided support to cell sorting. J.F. provided analytical pipelines and useful discussion for the analysis and normalization of mass cytometry data. S.G. and M.P. provided CAR constructs. C.J.T. provided expertise in mass cytometry and reagents. P.J.A. provided reagents and expertise and contributed to writing the manuscript. S.C. supervised the bioinformatic analyses and contributed to writing the manuscript. A.G. designed and supervised the project, performed and analyzed experiments and wrote the manuscript. All authors provided critical feedback and helped shape the research, analysis and manuscript.

**Non-author contributions and disclosures:** No;

**Agreement to Share Publication-Related Data and Data Sharing Statement:** Data will be shared through public repositories (GEO/ Github/ Cytobank) and sent by email upon request.

**Clinical trial registration information (if any):**

1 **Title**

2 **Activation priming and cytokine polyfunctionality modulate the enhanced functionality of low-**  
3 **affinity CD19 CAR T cells**

4 **Running title**

5 **Molecular profiling of low affinity CAR T-cells**

6

7 Ilaria M. Michelozzi<sup>1</sup>, Eduardo Gomez-Castaneda<sup>1\*</sup>, Ruben V.C. Pohle<sup>1\*</sup>, Ferran Cardoso Rodriguez<sup>2</sup>,  
8 Jahangir Sufi<sup>2</sup>, Pau Puigdevall Costa<sup>3</sup>, Meera Subramaniam<sup>1</sup>, Efstratios Kirtsios<sup>1</sup>, Ayad Eddaoudi<sup>1</sup>, Si  
9 Wei Wu<sup>1</sup>, Aleks Guvenel<sup>1</sup>, Jonathan Fisher<sup>4</sup>, Sara Ghorashian<sup>5</sup>, Martin A. Pule<sup>6</sup>, Christopher J. Tape<sup>2</sup>,  
10 Sergi Castellano<sup>3,7#</sup>, Persis J. Amrolia<sup>1,5#</sup> and Alice Giustacchini<sup>1</sup>.

11 1. Molecular and Cellular Immunology Section, UCL Great Ormond Street Institute of Child Health,  
12 London, UK

13

14 2. Cell Communication Lab, Department of Oncology, University College London Cancer Institute,  
15 London, UK

16

17 3. Genetics and Genomic Medicine Department, Great Ormond Street Institute of Child Health,  
18 University College London, London, UK

19

20 4. Developmental Biology and Cancer Section, UCL Great Ormond Street Institute of Child Health,  
21 London, UK

22

23 5. Department of Bone Marrow Transplant, Great Ormond Street Hospital for Children, London, UK

24

25 6. Cancer Institute, University College London, London, UK

26

27 7. UCL Genomics, Zayed Centre for Research into Rare Disease in Children, University College  
28 London, London, UK

29

30 \*These authors (E.G.C and R.V.C.P.) contributed equally to this work

31

#These authors (S.C. and P.J.A.) contributed equally to this work

32

Corresponding author: Alice Giustacchini, Zayed Centre For Research into Rare Disease in Children

33

UCL Great Ormond Street Institute of Child Health 20 Guilford Street, London WC1N 1DZ, email:

34

[a.giustacchini@ucl.ac.uk](mailto:a.giustacchini@ucl.ac.uk).

35

The RNA sequencing data and analyses are available at NCBI's Gene Expression Omnibus (GEO) data  
36 repository with the accession code GSE157584. Mass cytometry raw and processed data will be  
37 made publicly available at the Cytobank Community Servier (accession number 1481,

38 <https://community.cytobank.org> . For other forms of data sharing, contact the corresponding  
39 author: a.giustacchini@ucl.ac.uk.

40

#### 41 **Abstract**

42 We recently described a low-affinity second-generation CD19 chimeric antigen receptor (CAR) CAT  
43 that showed enhanced expansion, cytotoxicity, and anti-tumour efficacy compared to the high-  
44 affinity

45 (FMC63 based) CAR used in Tisagenlecleucel, in pre-clinical models. Furthermore, CAT  
46 demonstrated an excellent toxicity profile, enhanced *in vivo* expansion, and long-term persistence in  
47 a Phase I clinical

48 study. To understand the molecular mechanisms behind these properties of CAT CAR T-cells, we  
49 performed a systematic *in vitro* characterization of the transcriptomic (RNA-seq) and protein  
50 (CyTOF)

51 changes occurring in T-cells expressing low-affinity vs high-affinity CD19 CARs following stimulation  
52 with CD19-expressing cells. Our results show that CAT CAR T-cells exhibit enhanced activation to  
53 CD19 stimulation and a distinct transcriptomic and protein profile, with increased activation and  
54 cytokine polyfunctionality compared to FMC63 CAR T-cells. We demonstrate that the enhanced  
55 functionality of low-affinity CAT CAR T-cells is a consequence of an antigen-dependent priming  
56 induced by residual CD19-expressing B-cells present in the manufacture.

#### 57 **Key points**

58 • Low affinity CAT CAR T cells are characterized by a unique pattern of activation priming and  
59 cytokine polyfunctionality.

60 • The enhanced functionality of low-affinity CAT CAR T cells is a consequence of an antigen-  
61 dependent priming



63 **Regular Article**

64 **Introduction**

65 T-cells genetically engineered to express CD19 chimeric antigen receptors (CAR T-cells) have shown  
66 remarkable efficacy in relapsed/refractory (r/r) B-cell malignancies leading to clinical licensing for r/r  
67 B-cell acute lymphoblastic leukaemia (B-ALL) and Non-Hodgkin Lymphoma<sup>1</sup>. Despite this success,  
68 several safety and efficacy hurdles remain<sup>2</sup>. CAR T-cells can trigger potent immune responses leading  
69 to transient but potentially life-threatening inflammatory events, such as cytokine release syndrome  
70 (CRS) and neurotoxicity<sup>3,4</sup>. Thus, the design of versatile CAR T-cells, capable of balancing safety and  
71 efficacy, is contingent on our understanding of the molecular mechanisms underlying CAR T-cell  
72 function. The engagement of CARs to their cognate antigens results in the activation of CAR T-cells  
73 and promotes their rapid expansion as well as their differentiation into distinct T-cell subsets,  
74 mediating tumour cytotoxicity (effector cells) and providing long-lasting protection (memory cells). As  
75 tumour cell recognition by CAR T-cells relies on the binding of the CAR's single-chain variable  
76 fragment (scFv) to its epitope, fine-tuning the affinity of CARs to their antigens has become a  
77 strategy to modulate the strength of CAR T-cell responses<sup>5</sup>.

78

79 The affinity of CARs is determined by their binding kinetics and the rates at which they associate to  
80 and dissociate from their targets. The optimal affinity of a CAR is likely to vary depending on a  
81 number of factors, including the CAR design, the CAR expression levels and the antigen density on  
82 the target cells<sup>6,7</sup>. Chimeric immunoreceptors have an activation ceiling above which increasing the  
83 binding affinity does not improve T-cell activation but can rather result in T-cell exhaustion<sup>8</sup>. In  
84 contrast, by reducing CAR scFv affinity, the strength of the T-cell signal can be modulated, so that  
85 CAR T-cells discriminate different levels of antigen expression. CARs exhibiting slower antigen-  
86 association rates to ErbB2, EGFR and CD123 targets showed reduced activation in response to low  
87 antigen concentrations, favouring differential targeting of tumour cells overexpressing the target vs

88 normal tissue expressing the same target at physiological levels<sup>8-10</sup>. We have recently described a  
89 novel low-affinity CD19 CAR (CAT), with epitope, structure and stability similar to the widely used  
90 FMC63, but characterized by faster rates of antigen dissociation, leading to an overall 40-fold  
91 reduction of its affinity<sup>11</sup>. Pre-clinical testing of CAT CAR T-cells has revealed greater antigen-specific  
92 cytotoxicity, higher proliferation both *in vitro* and *in vivo* and more potent *in vivo* anti-tumour  
93 activity when compared to FMC63. In a Phase I clinical trial in patients with high-risk treatment-  
94 refractory paediatric B-ALL, CAT CAR T-cells resulted in lower toxicity in terms of severe CRS and  
95 displayed greater expansion than that reported for the FMC63 based tisagenlecleucel as well as  
96 excellent persistence<sup>11</sup>. These results were recently confirmed in a multicenter Phase I trial in r/r  
97 adult B-ALL<sup>12</sup>.

98

99 The molecular mechanisms through which the fine-tuning of CARs affinity influences CAR T-cell  
100 phenotypes and functions are largely unknown. The interaction between T-cell receptor (TCR) and  
101 the peptide-MHC complex offers however some insight on how immunoreceptors' affinity can  
102 dramatically influence T-cell functions<sup>13</sup>. Faster target off-rates in TCRs allow a single peptide-MHC  
103 complex to serially trigger several TCRs, resulting in amplified and sustained T-cell activation<sup>13</sup>.  
104 Similar to TCRs, low-affinity CARs may lead to enhanced T-cell activation and decreased exhaustion.  
105  
106 Herein we perform a systematic *in vitro* characterization of the molecular and biochemical changes  
107 occurring in CAR T-cells, comparing a low-affinity CD19 CAR (CAT) with a high-affinity one (FMC63).  
108 By combining bulk RNA sequencing with single-cell mass cytometry analyses (cytometry by time of  
109 flight, CyTOF), we show that the expression of the CAT CAR induces an antigen-dependent priming in  
110 response to low concentrations of CD19-expressing B-cells found in the manufacture product. Upon  
111 antigen stimulation, we identified distinct molecular features downstream of CAT CAR activation  
112 responsible for enhancing CAT CAR T-cell responses.

113

## 114 **Methods**

115

### 116 ***Ex vivo* T-cell expansion**

117 Freshly isolated PBMCs and CD19-depleted PBMCs were cultured in TexMACS<sup>TM</sup> medium (Miltenyi  
118 Biotec, Bergisch Gladbach, Germany), an optimised T-cell medium. To induce T-cell expansion,  
119 CD3/CD28 beads (CTS<sup>TM</sup> Dynabeads<sup>TM</sup> CD3/CD28, Thermo Fisher Scientific) were added to cells in  
120 MACS GMP Cell Differentiation Bags (Miltenyi Biotec) at a 1:3 lymphocyte:bead ratio. CD3/CD28  
121 beads were magnetically removed from the culture on day 5 and CAR T-cells rested for 48 h before  
122 proceeding to antigen stimulation.

123



124 **Lentiviral vector transduction**

125 Following overnight activation with CD3/CD28 beads,  $0.5 \times 10^6$  beads-activated T-cells were  
126 suspended in 0.5 ml of TexMACS, transduced to express CD19 CAR construct (FMC63 or CAT) with 1  
127 ml of LV supernatant in RetroNectin® (Takara Bio, Kusatsu, Shiga, Japan)-coated 24-well plates and  
128 spinoculated at 1,000 g for 40 min at room temperature. Generally,  $2-10 \times 10^6$  beads-activated T-cells  
129 per donor per construct were seeded for transduction.

130

131 **CAR T-cells co-cultures**

132 Briefly, beads-activated T-cells were incubated for 48 h in optimised T-cell medium before  
133 stimulation.  $0.1 \times 10^6$  UNTR or FMC63 or CAT beads-activated T-cells were seeded in 96-well plates in  
134 complete TexMACS medium in a 1:1 ratio with irradiated (40 Gy) NALM6. Generally,  $0.1-6 \times 10^6$   
135 beads-activated T-cells per donor per condition (UNTR, FMC63 and CAT) were stimulated.

136 Unstimulated, beads-activated T-cells per each donor, condition and time point were kept in culture  
137 under the same experimental conditions.

138

139 **Flow cytometry activated cell sorting and antibody staining**

140 All FACS experiments included Fluorescence minus one (FMO) and single-antibody stained BD™  
141 CompBeads (BD Biosciences) controls to set expression threshold and to calculate compensation,  
142 respectively. Experiments were performed on a cell sorter FACS Aria™ III (BD Biosciences) and on a  
143 CytoFLEX analyzer (Beckman Coulter Inc., Brea, CA, USA) and analysed with FlowJo™ software  
144 v10.6.1 (BD Biosciences) and Cytobank platform ([www.cytobank.org](http://www.cytobank.org)). Details on the antibody panels  
145 can be found in the Supplementary Methods.

146

147 **Mass cytometry analysis**

148 Following 24 h of stimulation, samples in all experimental conditions were treated with Brefeldin A  
149 (BioLegend) (1:1,000) at 37°C for 4 h to favour intracellular cytokine accumulation and were fixed

150 with 1.6% of formaldehyde for 10 min at room temperature. Fixed samples were processed,  
151 barcoded (Cell-ID™ 20-Plex Pd Barcoding Kit, Fluidigm) and stained as previously described<sup>14</sup>. Two  
152 independent mass cytometry experiments were performed and the antibodies used are listed in  
153 Supplementary Table 3. The samples were analyzed on a Helios mass cytometer (Fluidigm). EQ™  
154 Four Element Calibration Beads (Fluidigm) were added to cell suspensions immediately before  
155 acquisition to guarantee inter-sample comparability.

156

### 157 **Statistical analyses**

158 Data are shown as mean ± standard error (se) and statistical analyses were performed in R  
159 calculating Paired samples t-tests across experimental conditions unless otherwise stated.  
160 EMD-related statistical analyses between selected experimental conditions and the results of  
161 polyfunctionality analysis are reported in Supplementary Table 5.

162

### 163 **Data availability**

164 The RNA sequencing data and analyses are available at NCBI's Gene Expression Omnibus (GEO) data  
165 repository with the accession code GSE157584 and in GitHub  
166 ([https://github.com/EduardoGCCM/CATvsFMC63\\_Michelozzi](https://github.com/EduardoGCCM/CATvsFMC63_Michelozzi)).

167 Mass cytometry raw and processed data will be made publicly available at  
168 <https://community.cytobank.org/>.

### 169 **Results**

#### 170 **Generation and quality assessments of low- (CAT) and high- (FMC63) affinity CD19 CARs from** 171 **healthy donors**

172 To dissect the molecular mechanisms behind the functional differences observed between low-  
173 (CAT) and high- (FMC63) affinity CD19 CAR T-cells<sup>11</sup>, we interrogated the transcriptional and protein  
174 expression profiles of T-cells lentivirally (LV) transduced with CARs differing only in their scFv

175 (Supplementary Figure 1A). We performed bulk transcriptomic analyses (RNA-seq) to identify CAR T-  
176 cell distinct gene expression signatures and mass cytometry analyses (CyTOF) to model differences  
177 in their downstream signalling at a single-cell resolution<sup>14</sup>. RNA-seq and CyTOF readouts from  
178 untransduced (UNTR) controls and T-cells LV transduced to express CAT or FMC63 CD19 CARs from  
179 healthy donors (HD1-HD27, Supplementary Table 1) were compared at baseline and following  
180 stimulation with CD19+ ALL cell line NALM6 (unstimulated and stimulated conditions, respectively),  
181 as schematized in Figure 1A. We ruled out significant differences in the transduction of the two CARs  
182 by fluorescence activated cell sorting (FACS), assessing the percentage of mCherry+ T-cells (LV  
183 fluorescent reporter) across donors and experimental conditions. These ranged between 11.50 -  
184 93.80% (median 39.1%) in FMC63 and 13.40 - 93.60% (median 36.25%) in CAT (Figure 1B, left) and  
185 were thus comparable among individual HDs. In agreement, we found similar transgene expression  
186 levels between the 2 CARs by measuring mCherry mean fluorescent intensity (MFI), a proxy for CARs  
187 expression (Figure 1B, right) and by quantifying CARs surface expression levels (Figure 1C) and  
188 number of integrated vector copies (VCN) (Supplementary Figure 1B). Finally, we assessed CAT and  
189 FMC63 CAR T-cell products for their CD4:CD8 ratios and memory T-cell subsets composition, as  
190 these characteristics can both affect CAR T-cells persistence and anti-tumour activity<sup>15,16</sup>. While no  
191 difference in CD4:CD8 ratios was observed in the absence of antigen stimulation (Figure 1D), the  
192 proportion of memory subsets differed in unstimulated FMC63 and CAT CAR T-cells, as measured by  
193 FACS at 10 days post-transduction. CAT CAR T-cells exhibited a significant increase in the fraction of  
194 central memory T-cells ( $T_{CM}$ , CD62+CD45RA-) as compared to both UNTR and FMC63 conditions  
195 (Figure 1E, left). The increase in  $T_{CM}$  was largely at the expense of T effector memory cells ( $T_{EM}$ , CD62-  
196 CD45RA-) and effector memory re-expressing CD45RA ( $T_{EMRA}$ , CD62-CD45RA+), whose proportion  
197 was significantly reduced in CAT vs FMC63 CAR T-cells and in both CARs as compared to UNTR  
198 control (Figure 1E, middle and right). These assessments confirmed that our CAR T-cell products  
199 were suitable to investigate the molecular features of CAT and FMC63 CAR T-cells.

200

## 201 **Low-affinity CD19 CARs display higher activation priming during CAR T cell manufacture**

202 We next performed bulk RNA-seq of FACS-sorted UNTR T-cells (CD3+) and FMC63 or CAT CAR T-cells  
203 (CD3+mCherry+) with or without a 24 h stimulation with NALM6. Transcriptomics confirmed that  
204 mCherry was an accurate proxy for CAR transgene expression levels, as evidenced by the significant  
205 positive correlation between the MFI of mCherry by FACS and the normalized RNA-seq counts  
206 aligning to the scFv region of each of the 2 CARs (Supplementary Figure 2A). Similarly, the proportion  
207 of CD4 and CD8 T-cells detected by FACS was in line with the *CD4* and *CD8* mRNA levels  
208 (Supplementary Figure 2B, C). Principal component analysis (PCA) on the 500 most variable  
209 expressed genes (top 100 genes shown in Supplementary Figure 2D), distributed samples according  
210 to a T-cell activation gradient (PC1, from UNTR to CAR activated samples) (Figure 2A). The majority  
211 of variance in gene expression across experimental conditions was explained by CD19-mediated CAR  
212 activation. As expected, UNTR T-cells not expressing any CARs were largely unaffected by antigen  
213 stimulation (Figure 2A). Similarly, PCA on protein expression from CyTOF, based on earth mover's  
214 distance (EMD) scores (a sensitive measure of multivariate changes in protein levels)<sup>17</sup>, in the same  
215 experimental conditions and timepoints than the gene expression, followed a similar gradient of  
216 sample activation, shifting from UNTR samples to antigen stimulated CAR T-cells on PC1 (Figure 2B  
217 and Supplementary Figure 3A). The most variable genes upregulated upon stimulation with NALM6  
218 in both FMC63 and CAT CAR T-cells included genes involved in T-cell activation (*IL2RA*, *GZMB*) and  
219 proliferation (*PCNA*, *LDHA*), which are expressed at very low levels in control T-cells (Supplementary  
220 Figure 2D). Consistent with this, the highest protein expression variation was from markers of T-cell  
221 activation (CD25, NFAT1, HLA-DR) and proliferation (pRB) (Supplementary Figure 3A). In both RNA  
222 and protein analyses, unstimulated CAR T-cells had an intermediate RNA/protein expression profile  
223 between UNTR and stimulated CAR T-cells. This suggests that CAR expression on its own, in absence  
224 of antigen stimulation, induces basal T-cell activation (Figure 2A-B).

225

226 To gain further insights into the intermediate activation state observed in unstimulated CAR T-cells,  
227 we fuzzy clustered individual samples by their gene expression, to resolve intermediate cell states  
228 and trajectories (Figure 2C)<sup>18</sup>. We identified two clusters, highly enriched for either inactive T-cells  
229 (cluster 1, which includes UNTR samples) or antigen-activated CAR T-cells (cluster 2, which includes  
230 stimulated CAR T samples) (Figure 2C). Notably, the probability of unstimulated CAT samples of  
231 belonging to cluster 2 (activated CAR T-cells) was substantially higher than that of unstimulated  
232 FMC63 (4/6 HDs in CAT vs 0/6 HDs in FMC63), further evidencing the functional proximity between  
233 unstimulated CAT and activated CAR T-cells. Using gene set enrichment analyses (GSEA) on the  
234 Hallmark collection, we confirmed that while antigen stimulated CAT and FMC63 CAR T-cells have  
235 similar enrichment for most of the gene sets involved in immune functions and cell proliferation, in  
236 the absence of antigen stimulation CAT CAR T-cells are uniquely enriched for T-cell activation  
237 pathways (Supplementary Figure 3B).

238 Next, we compared the transcriptome of FMC63 and CAT CAR T-cells, in absence of antigen  
239 stimulation. Following differential gene expression (DGE) analysis, we found that only 10 genes were  
240 significantly DE between these two conditions (FDR < 0.1, Supplementary Table 2), 9 of which were  
241 upregulated in CAT vs FMC63 CAR T-cells. Among those, we found genes involved in cytotoxicity  
242 (*GNLY*, *GZMK*) and markers of T-cell activation such as MHC class II molecules (MHCII) (*HLA-DRA* and  
243 *HLA-DPA*) (Figure 2D). This supports our previous observation of gene expression in unstimulated  
244 CAT resembling more that of antigen activated CAR T-cells than gene expression in unstimulated  
245 FMC63 (Figure 2C). Mass cytometry analyses using a panel of antibodies against markers of T-cell  
246 activation (Supplementary Table 3), confirmed that while unstimulated FMC63 and CAT CAR T-cells  
247 have similar EMD scores for many of the proteins investigated (Supplementary Table 5a),  
248 unstimulated CAT CAR T-cells have significantly stronger activation priming with higher expression of  
249 markers of T-cell activation (HLA-DR, CD25 and NFAT1), pro-inflammatory (Granzyme B, Perforin B)  
250 and stimulatory/activation-related (GM-CSF, IL-17A) cytokines and increased phosphorylation of the

251 TCR/CAR CD3 $\zeta$  chain (pZAP70) and MTOR downstream effector (pS6) (Figure 2E and Supplementary  
252 Figure 3C).

253 Altogether, these results show that unstimulated CAT CAR T-cells, prior to antigenic stimulation,  
254 have more pronounced T-cell activation priming than FMC63 CAR T-cells.

255

256 **CD19 stimulation of low-affinity CAT CAR T-cells results in a distinct transcriptomic and protein**  
257 **profile with increased activation/proliferation over high-affinity FMC63 CAR T-cells**

258 While antigen-independent CAR activation, also known as tonic signalling, has been often associated  
259 with CAR T-cell accelerated differentiation and exhaustion<sup>19-21</sup>, recent data show that the induction  
260 of CAR T-cell priming can lead to CAR T enhanced anti-tumour functions *in vivo*<sup>22,23</sup>. We wanted to  
261 assess the molecular impact of the “activation priming” observed in CAT CAR T-cells on their  
262 molecular response to antigen stimulation. As the superior cytotoxicity of CAT CAR T-cells over  
263 FMC63 CAR T-cells has been previously shown in functional assays<sup>11</sup>, we focused on characterizing  
264 their distinct molecular profiles upon exposure to antigenic stimulation. Upon stimulation, we found  
265 a slight but statistically significant reduction of CD4:CD8 ratio in CAT as compared to FMC63 (Figure  
266 3A), largely attributable to a relative decrease of the CD8+ fraction (and increase of CD4+) in FMC63  
267 CAR T-cells (Supplementary Figure 4A). Interestingly, when looking at the memory T-cell subsets  
268 composition, we found that CAT CAR T-cells continued to exhibit a higher proportion of T<sub>CM</sub> as  
269 compared to FMC63 (Figure 3B), while no differences were observed in the expression of exhaustion  
270 markers (PD1, TIM3 and LAG3) between the two CAR constructs (Figure 3C).

271 Importantly, the stronger basal activation observed in CAT CAR T-cells did not prevent an even  
272 stronger molecular response when exposed to CD19-expressing NALM6, as shown by the increase in  
273 the expression of proliferation and cytotoxic/stimulatory markers, relatively to the unstimulated  
274 constructs (Supplementary Figure 5 and 6). Consistent with this, we identified 51 DE genes, 35 of  
275 which were upregulated in CAT compared to FMC63 (Figure 3D and Supplementary Table 4). CD19

276 stimulation in CAT CAR T-cells also led to significantly augmented expression of immune  
277 stimulatory/proliferation cytokines (*IFNG*, *CSF2*, *CXCL8*), and IFN- $\gamma$  responsive genes (*CIITA*) (Figure  
278 3D and Supplementary Figure 4B). Conversely, CAT CAR T-cells displayed significantly decreased  
279 expression of the genes encoding for CRIF1 (*GADD45GIP1*), an inhibitor of cell cycle progression, and  
280 for FOXP3, the Treg-associated transcription factor known to be only transiently expressed in the  
281 initial stages of Th1 response and rapidly downregulated afterwards<sup>24,25</sup> (Figure 3D). These results  
282 suggest that following antigenic stimulation CAT CAR T-cells show a different transcriptomic profile  
283 resulting in stronger activation and proliferation than stimulated FMC63. In addition, CAT CAR T-cells  
284 showed increased expression of the *TNFSF4* gene (Figure 3D), encoding for the ligand of the T-cell  
285 co-stimulatory receptor OX40 (OX40L). While OX40L is mainly expressed by antigen presenting cells  
286 to promote T-cell activation, it is also expressed in activating T-cells, where it leads to a homotypic  
287 OX40L-OX40 signalling axis promoting T-cell longevity and memory differentiation<sup>26</sup>. Further, we also  
288 noted the increased expression of the chemoattractants *CCL4* and *CCL3L1* and genes involved in cell  
289 migration (*FLT1*, *DOCK5*) and focal adhesion (*COL6A3*) in stimulated CAT CAR T-cells (Supplementary  
290 Figure 4B).

291 These observations were further substantiated at the protein level. CAT CAR T-cells exhibited a  
292 marked increase in the expression (as measured by EMD score) of markers of T cell activation (CD25)  
293 (Figure 3E). Moreover, the augmented gene expression of the MHCII trans-activator *CIITA* observed  
294 in CAT, resulted in a corresponding increase of HLA-DR protein (Figure 3E)<sup>27,28</sup>. When measuring the  
295 CAR T-cell intracellular signalling, CAT CAR T-cells showed enhanced phosphorylation of the effectors  
296 of the TCR/CAR CD3 $\zeta$  chain (pZAP70, pp38) and increased expression of their downstream  
297 transcription factors (NFAT1, pCREB, FOXP3). CAT CAR T-cells also exhibited significant upregulation  
298 of the Target of Rapamycin Complex 1 (mTORC1) downstream effectors (pS6 and pRB), both  
299 involved in cell proliferation and protein translation, in line with the previously reported CAT CAR T  
300 cells increased proliferative capacity over FMC63<sup>11</sup>.

301 Our analysis shows that the increased “activation priming” observed in CAT CAR T-cells over FMC63  
302 resulted in an even stronger T-cell activation gene expression and signaling profile when CAT CAR T-  
303 cells were exposed to antigenic stimulation. These observations are in line with the CAT CAR T cells  
304 enhanced cytotoxic functional properties previously reported<sup>11</sup>.

305 **The enhanced functionality of low-affinity CD19 CAR T-cells is associated with cytokine**  
306 **polyfunctionality upon antigen stimulation**

307 We next assessed CAR T-cell functional phenotypes by measuring intracellular cytokines levels in  
308 individual cells by mass cytometry. The overall protein intensities measured by EMD scores indicated  
309 an increased expression of effector cytokines (Granzyme B , IFN- $\gamma$  and TNF- $\alpha$ ) and of immune  
310 stimulatory molecules (GM-CSF and IL-2) in CAT CAR T as compared to FMC63 (Figure 4A). No  
311 upregulation was observed for Th2/immune-modulatory cytokines (IL-4, IL-5 and TGF- $\beta$ ) and for  
312 Perforin B (Supplementary Table 5b).

313

314 Next, we investigated the pattern of cytokine co-expression in CAT and FMC63 CAR T-cell responses.  
315 The ability of a single T-cell to express simultaneously more than one cytokine (polyfunctionality) has  
316 been linked to productive immune responses<sup>29,30</sup> and more recently described as a distinctive  
317 feature of CAR T-cells associated to their potency and anti-tumour efficacy<sup>31-33</sup>. We measured the  
318 frequency at which the eight cytokines included in our analysis were co-expressed in single CAR T-  
319 cells, thus providing a comprehensive profile of their cytokine polyfunctionality. Upon stimulation  
320 with NALM6, 15.02% of FMC63 and 29.60% of CAT CAR T-cells were polyfunctional (expressing two  
321 or more cytokines per cell) (Supplementary Table 5n).

322 Not only the frequency of polyfunctional CAR T-cells, but also the number of cytokines co-expressed  
323 was higher in CAT than in FMC63, with a statically significant increase in their mean  
324 polyfunctionality (Figure 4B) and a marked increment in the proportion of cells expressing  
325 combinations of three or more cytokines (2.28% in FMC63 vs 7.89% in CAT) (Figure 4C and



326 Supplementary Table 5o). The polyfunctional profiles of stimulated CAT CAR T-cell products were  
327 dominated by combinations of cytokines involving the effector molecules IFN-g, TNF- $\alpha$ , IL-2 and  
328 Granzyme B (Figure 4D).

329 **Low-affinity CD19 CAR activation priming is associated with and driven by residual CD19-**  
330 **expressing B-cells**

331 To investigate whether the mechanism behind the activation priming observed in unstimulated CAT  
332 CAR T-cells was antigen-dependent or -independent, we checked if residual CD19+ B-lymphocytes  
333 were detectable in the CAR T-cell product and could serve as a potential source of antigen specific  
334 activation.

335

336 We monitored the proportion of CD19+ B-lymphocytes in culture at different timepoints. While B-  
337 cells were detectable at day 0 in all samples (5.96% of cells on average), at day 8 (5 day stimulation  
338 with CD3/CD28 beads + 3 day rest) they could only be detected in the UNTR condition (2.33% of cells  
339 on average), and had been completely depleted from both CAR constructs, as shown by FlowSOM  
340 analysis of mass cytometry data, clustering single-cells by cell types<sup>34</sup>, and the relative frequencies  
341 (Figure 5A and Supplementary Figure 7A). We next applied the experimental setup described in  
342 Figure 1A, only now including as additional experimental condition CAR T-cells generated from  
343 CD19-depleted PBMCs. We confirmed effective CD19 depletion by flow cytometry, with an average  
344 of residual B cells of 0.041% upon depletion as compared to 5.96% with the standard protocol  
345 (Supplementary Figure 7B). The transduction levels obtained in the CD19-depleted CAT and FMC63  
346 CAR T-cells were comparable based on the expression of the fluorescent reporter (mCherry) and the  
347 VCN (Supplementary Figure 7C-D). The baseline CD4:CD8 ratios only showed a slight increase in CAT  
348 as compared to FMC63 CAR T cells (Supplementary Figure 7E). Of note, CD19-depletion impacted on  
349 the T memory subsets composition, with CAT CAR T-cells no longer displaying any statistical

350 difference when compared to the UNTR control, while FMC63 CAR T-cells still showing a significant  
351 increase in the proportion of T<sub>EM</sub> when compared to the UNTR control (Figure 5B).

352 Mass cytometry analyses revealed that the residual B cells in the CAR T-cell manufacture were  
353 responsible for the activation priming observed in unstimulated CAT and FMC63 CAR T-cells  
354 (Supplementary Figure 8, 9). While CD19 depletion led to a general decrease in the activation  
355 priming previously observed in unstimulated CAR T-cells, this reduction was more pronounced in  
356 CAT (Supplementary Figure 8) than in FMC63 (Supplementary Figure 9). As a result, upon B cell  
357 depletion we no longer detected statistically significant differences in the expression of T-cell  
358 activation markers (HLA-DR, CD25 and NFAT1), pro-inflammatory cytokines (Granzyme B, Perforin B)  
359 and CAR-downstream signaling molecules (pZAP70 and pS6) between CAT and FMC63 (Figure 5C).  
360 Differential protein expression between CD19-depleted CAT and FMC63 CAR T-cells was only  
361 observed for pRB and CD69 (Supplementary Figure 7F). Both CAT and FMC63 CAR T cells exhibited  
362 increased expression of activation and cytotoxic markers with respect to the UNTR controls they are  
363 normalized to, indicating similar levels of antigen-independent activation (Figure 5C).

364 When later exposed to NALM6, both CD19-depleted CAT and FMC63 were able to activate, as shown  
365 by the upregulation of the expression of cytotoxic markers and cytokines compared to their  
366 unstimulated counterparts (Supplementary Figure 10, 11). No differences in the CD4:CD8 ratios and  
367 in the expression of exhaustion markers were observed between the two stimulated CAR conditions  
368 upon CD19-depletion (Supplementary Figure 7G, H). Most importantly, upon antigenic stimulation,  
369 CD19-depleted CAT CAR T-cells activated a molecular response with no statistically significant  
370 differences when compared to FMC63 (Figure 5D and Supplementary Figure 7I), except for an  
371 increased expression of IL-2 (Supplementary Figure 7I). The increased cytokine polyfunctionality  
372 observed in CAT vs FMC63 CAR T-cells in standard manufacture condition (Figure 4) was no longer  
373 observed in CD19-depleted manufacture condition (Figure 5E).

374

375 Altogether these results demonstrate that residual B-cells in the CAR T-cell manufacture can  
376 mediate an antigen dependent activation priming, which is more pronounced in low affinity CAT CAR  
377 T-cells when compared to FMC63 CAR T-cells. Such activation priming contributes to boosting CAT  
378 CAR T-cell response, as CAT CAR T-cells generated from CD19-depleted PBMCs not only do not  
379 display increased activation priming but also do not exhibit increased molecular responses to  
380 antigenic stimulation with NALM6.

### 381 **Discussion**

382 Modulating CAR T-cell affinity may enable us to enhance anti-tumour response and long-term  
383 tumour surveillance, while minimizing CAR T-cell related toxicity. We thus investigated the  
384 transcriptomic and proteomic phenotype of CD19 CAT CAR T-cells, compared with the widely used  
385 FMC63, to begin unravelling the molecular mechanisms behind the observed preclinical and clinical  
386 differences between these two CD19 CARs<sup>11</sup>.

387 We found that CAT CARs induce stronger activation responses than FMC63, which could be  
388 explained by the faster target off-rate of low-affinity CARs. Faster dissociation requires fewer targets  
389 to serially trigger a larger number of CARs and amplify anti-tumoural response<sup>13</sup>. This would align  
390 with the proposed model of temporal and spatial summation of T-cell activation, in which signals  
391 from serially triggered immunoreceptors can be accumulated and integrated overtime to reach the  
392 threshold required for T-cell activation<sup>35</sup>. This model may also explain why low levels of residual  
393 donor B cells in the manufacture can induce stronger activation priming in CAT CAR T cells than in  
394 FMC63.

395 Our transcriptomic and protein profiling revealed that unstimulated CAT CAR T-cells are functionally  
396 closer to antigen activated CAR T-cells than FMC63 CAR T-cells, with a number of upregulated  
397 activation genes (*HLA-DBP1*, *HLA-DRA* etc) and proteins (*HLA-DR*, *CD25* and *NFAT1*). Despite these  
398 genes/proteins being commonly associated to T-cell activation, their basal expression is also  
399 increased in memory T-cells as compared to T<sub>NAÏVE</sub> cells, as memory T-cells are characterized by an

400 open chromatin conformation favouring the access of transcription factors to immune response  
401 genes, thus ensuring a pool of readily available mRNAs that can be rapidly translated following  
402 stimulation<sup>36</sup>. This hypothesis is in agreement with the increased proportion of T<sub>CM</sub> observed in CAT  
403 CAR T cells as compared to FMC63. However, further studies are needed to elucidate the molecular  
404 signalling underlying the preferential differentiation towards T<sub>CM</sub> in low-affinity CAT CAR T-cells.

405

406 By performing B cell depletion prior to CAR T-cell manufacture, we demonstrate that residual B-cells  
407 in the CAR T-cell product are responsible for the activation priming observed in CAR T-cells, which  
408 was more pronounced in CAT when compared to FMC63, and preferentially induce T<sub>CM</sub>  
409 differentiation of CAT CAR T-cells. This is consistent with the hypothesis that CAT serial triggering  
410 may amplify T-cell activation from lower antigen levels<sup>13</sup> and points to a boosting role of low dose  
411 CD19-priming during CAR T-cell manufacture. The preferential T<sub>CM</sub> phenotype in CAT CAR T-cells  
412 might be due to kinetic differences in clearance of residual B cells or to different downstream  
413 signalling after antigenic stimulation with low- vs high-affinity CAR T-cells. Further work elucidating  
414 these mechanisms is needed. Recent results have shown that antigen-independent induction of CAR  
415 T-cell priming, by either 4-1BB-based tonic signalling<sup>22</sup> or by low-dose of hypomethylating agents<sup>23</sup>,  
416 can lead to enhanced CAR T anti-tumour functions *in vivo* and it is regulated by the recruitment of  
417 LCK or THEMIS-SHP1 phosphatase into the CAR synapse<sup>37</sup>. Our results indicate that low dose  
418 antigen-specific priming can also promote CAR T-cell functionality in a CAR construct specific manner  
419 with an enhanced effect in low-affinity CAR T-cells.

420

421 When stimulated with CD19-expressing NALM6 cell line, CAT CAR T-cells have a distinct  
422 transcriptomic and protein response to CD19 antigenic stimulation from FMC63 CAR T-cells with  
423 increased expression of proliferation, activation and cytotoxic markers at both RNA and protein  
424 levels. *In vivo* clonal kinetics analyses have shown that single CD19 CAR T-cells with higher

425 expression of cytotoxic related genes in the manufacture product, many of which in common with  
426 ours (including *IFNG*, *HLA-DRA*, *CCL4*), gave rise to superior *in vivo* expansion and survival,  
427 significantly contributing to later timepoints after adoptive transfer in patients<sup>19,38</sup>. Analysis of gene  
428 expression also revealed the upregulation of chemoattractive cytokines CCL4 and CCL3L1 in CAT,  
429 which induce T-cell homotypic interactions and promote the reciprocal exchange of self-reinforcing  
430 signals such as OX40L,<sup>26,39</sup> which are upregulated in CAT as well. Single-cell transcriptomic studies  
431 have revealed that subsets of CAR T with elevated expression of CCL3 and CCL4 are associated to  
432 longer persistence *in vivo*<sup>38</sup> and achievement of complete remission<sup>40</sup>. Mass Cytometry analyses  
433 revealed a CAT CAR T enhanced activation protein profile, as measured by the increased expression  
434 of T-cell activation markers (CD25, HLA-DR) and CAR downstream signaling effectors (pZAP70, pp38,  
435 NFAT1, pCREB, FOXP3). Furthermore, CAT CAR T-cells showed increased mTORC signaling (pS6 and  
436 pRB), which is commonly associated to cell proliferation and protein translation. Altogether, CAT  
437 CAR T-cells distinct gene expression and protein profiles are very much in line and likely responsible  
438 for the enhanced proliferative responses that CAT CAR T-cells exhibited *in vitro*, in *in vivo* murine  
439 models and in patients, as previously reported by Ghorashian et al.<sup>11</sup>.

440

441 Upon stimulation, CAT CAR T-cells were characterized by a unique polyfunctional pattern of cytokine  
442 expression, with a marked increase in the frequency of single CAR T-cells expressing  $\geq 3$  cytokines  
443 when compared to FMC63. CAT polyfunctional profile was dominated by combinations of effector  
444 cytokines, consistent with their potent anti-tumour activity. It has been suggested that the ability of  
445 CAR T-cells to produce multiple cytokines in response to antigen exposure is associated with  
446 improved anti-tumour responses *in vivo*<sup>31</sup> and cytokine polyfunctionality has been recently proposed  
447 as a criteria to predict CAR T-cell potency<sup>33</sup>. The increased cytokine polyfunctionality observed in  
448 CAT CAR T-cells contributes to explain their increased cytotoxic potential previously observed *in vitro*  
449 *settings* and in *in vivo* murine models<sup>11</sup>.

450

451 In conclusion, we describe the molecular mechanisms underlying the low-affinity CAT CAR T-cell  
452 functional phenotype. We provide evidence that the potent and long-term anti-tumour responses  
453 observed with low-affinity CAT CAR T-cells<sup>11</sup> reflect a distinct pattern of both activation priming and  
454 cytokine polyfunctionality. We show that low-affinity CAT CAR T-cells are preferentially primed by  
455 low concentration of CD19-expressing B-cells present in the manufacture and such priming is  
456 instrumental to their higher cytotoxic response upon stimulation. Although our observations are  
457 limited to one low-affinity CAR, future work extending this characterization to a panel of low-affinity  
458 CARs, may reveal whether these findings are generalisable. In future work, we will focus on  
459 elucidating the mechanism by which residual B cells in the starting material induce  
460 differential effects on low vs high affinity CAR T-cells and whether there is a dose-  
461 dependent relationship between residual CD19+ B cells and CAR T-cell functionality. This will  
462 have important implications for CAR T-cell manufacturing protocols.

463 Overall, our work has important implications for the future design of versatile CAR T-cells  
464 manufacture protocols, capable of boosting efficacy and long-term persistence.

465

#### 466 **Acknowledgements**

467 We are grateful to the UCL ICH Flow Cytometry facility for support in cell-sorting. We are grateful to  
468 Dr Thomas Adejumo (Fluidigm) for mass cytometry valuable suggestions and assistance with  
469 protocols design. We thank Dr Anne Marijn Kramer (Amsterdam UMC) for generating CD19 FMC63  
470 and CAT CAR transfer vector plasmids with S.G. and M.P. and P.J.A. The authors acknowledge the  
471 contribution of UCL Genomics Facility. This work was supported by the NIHR GOSH BRC (NIHR GOSH  
472 BRC 17PA01), the views expressed are those of the author(s) and not necessarily those of the NHS,  
473 the NIHR, or the Department of Health. Part of this work was supported by the Leukaemia UK John  
474 Goldman Fellowship to A.G. (2018/JGF/003), the Rosetrees Trust fund to A.G. (M700) and the  
475 Academy of Medical Sciences Springboard Award to A.G. (SBF004\1025).

476

#### 477 **Authorship**

478 Contributions: I.M.M. designed, performed and analyzed experiments, performed bioinformatic  
479 analyses of mass cytometry experiments and contributed to writing the manuscript. E.G-C  
480 performed bioinformatic analyses of transcriptomic data and wrote the relative bioinformatic  
481 supplementary information. R.V.C.P. performed experiments and bioinformatic analyses of mass  
482 cytometry and transcriptomic data. F.C-R provided data analysis tools and contributed to  
483 bioinformatic analyses of mass cytometry experiments. P.P-C. performed transcriptomic  
484 bioinformatic analyses data checks and contributed to writing the bioinformatic supplementary  
485 information. J. S., M.S., S.W.W, A.Gu. and E.K. performed experiments. A.E. provided support to cell  
486 sorting. J.F. provided analytical pipelines and useful discussion for the analysis and normalization of  
487 mass cytometry data. S.G. and M.P. provided CAR constructs. C.J.T. provided expertise in mass  
488 cytometry and reagents. P.J.A. provided reagents and expertise and contributed to writing the  
489 manuscript. S.C. supervised the bioinformatic analyses and contributed to writing the manuscript.  
490 A.G. designed and supervised the project, performed and analyzed experiments and wrote the  
491 manuscript. All authors provided critical feedback and helped shape the research, analysis and  
492 manuscript.

493 Conflict of Interest: S.G. received speaker's honoraria from Novartis and patents and royalties from  
494 UCLB. M.A.P. owns stock in and is in part employed by Autolus Therapeutics, that has licensed CAT  
495 CAR. P.J.A. has received Royalties for a patent related to CAT CAR from Autolus and receives  
496 research funding from Autolus. The remaining authors declare no competing interests.

497

498 **Correspondence: Alice Giustacchini**, Zayed Centre For Research into Rare Disease in Children  
499 UCL Great Ormond Street Institute of Child Health 20 Guilford Street, London WC1N 1DZ, email:  
500 [a.giustacchini@ucl.ac.uk](mailto:a.giustacchini@ucl.ac.uk)

501 **References**

502

- 503 1. Miliotou AN, Papadopoulou LC. CAR T-cell Therapy: A New Era in Cancer  
504 Immunotherapy. *Curr Pharm Biotechnol*. 2018;19(1):5-18.
- 505 2. Pehlivan KC, Duncan BB, Lee DW. CAR-T Cell Therapy for Acute Lymphoblastic  
506 Leukemia: Transforming the Treatment of Relapsed and Refractory Disease. *Curr Hematol*  
507 *Malig Rep*. 2018;13(5):396-406.
- 508 3. Lee DW, Gardner R, Porter DL, et al. Current concepts in the diagnosis and  
509 management of cytokine release syndrome. *Blood*. 2014;124(2):188-195.
- 510 4. Gust J, Hay KA, Hanafi LA, et al. Endothelial Activation and Blood-Brain Barrier  
511 Disruption in Neurotoxicity after Adoptive Immunotherapy with CD19 CAR-T Cells. *Cancer*  
512 *Discov*. 2017;7(12):1404-1419.
- 513 5. Watanabe K, Kuramitsu S, Posey AD, Jr., June CH. Expanding the Therapeutic  
514 Window for CAR T Cell Therapy in Solid Tumors: The Knowns and Unknowns of CAR T  
515 Cell Biology. *Front Immunol*. 2018;9:2486.
- 516 6. Kowolik CM, Topp MS, Gonzalez S, et al. CD28 costimulation provided through a  
517 CD19-specific chimeric antigen receptor enhances in vivo persistence and antitumor efficacy  
518 of adoptively transferred T cells. *Cancer Res*. 2006;66(22):10995-11004.
- 519 7. Singh AP, Zheng X, Lin-Schmidt X, et al. Development of a quantitative relationship  
520 between CAR-affinity, antigen abundance, tumor cell depletion and CAR-T cell expansion  
521 using a multiscale systems PK-PD model. *MAbs*. 2020;12(1):1688616.
- 522 8. Chmielewski M, Hombach A, Heuser C, Adams GP, Abken H. T cell activation by  
523 antibody-like immunoreceptors: increase in affinity of the single-chain fragment domain  
524 above threshold does not increase T cell activation against antigen-positive target cells but  
525 decreases selectivity. *J Immunol*. 2004;173(12):7647-7653.
- 526 9. Caruso HG, Hurton LV, Najjar A, et al. Tuning Sensitivity of CAR to EGFR Density  
527 Limits Recognition of Normal Tissue While Maintaining Potent Antitumor Activity. *Cancer*  
528 *Res*. 2015;75(17):3505-3518.
- 529 10. Liu X, Jiang S, Fang C, et al. Affinity-Tuned ErbB2 or EGFR Chimeric Antigen  
530 Receptor T Cells Exhibit an Increased Therapeutic Index against Tumors in Mice. *Cancer*  
531 *Res*. 2015;75(17):3596-3607.
- 532 11. Ghorashian S, Kramer AM, Onuoha S, et al. Enhanced CAR T cell expansion and  
533 prolonged persistence in pediatric patients with ALL treated with a low-affinity CD19 CAR.  
534 *Nat Med*. 2019;25(9):1408-1414.
- 535 12. Roddie C, Dias J, O'Reilly MA, et al. Durable Responses and Low Toxicity After Fast  
536 Off-Rate CD19 Chimeric Antigen Receptor-T Therapy in Adults With Relapsed or  
537 Refractory B-Cell Acute Lymphoblastic Leukemia. *J Clin Oncol*. 2021:JCO2100917.
- 538 13. Valitutti S, Muller S, Cella M, Padovan E, Lanzavecchia A. Serial triggering of many  
539 T-cell receptors by a few peptide-MHC complexes. *Nature*. 1995;375(6527):148-151.
- 540 14. Michelozzi IM, Sufi J, Adejumo TA, Amrolia PJ, Tape CJ, Giustacchini A. High-  
541 dimensional functional phenotyping of preclinical human CAR T cells using mass cytometry.  
542 *STAR Protoc*. 2022;3(1):101174.
- 543 15. Wang X, Popplewell LL, Wagner JR, et al. Phase 1 studies of central memory-derived  
544 CD19 CAR T-cell therapy following autologous HSCT in patients with B-cell NHL. *Blood*.  
545 2016;127(24):2980-2990.
- 546 16. Wang X, Wong CW, Urak R, et al. Comparison of naive and central memory derived  
547 CD8(+) effector cell engraftment fitness and function following adoptive transfer.  
548 *Oncoimmunology*. 2016;5(1):e1072671.



- 549 17. Orlova DY, Zimmerman N, Meehan S, et al. Earth Mover's Distance (EMD): A True  
550 Metric for Comparing Biomarker Expression Levels in Cell Populations. *PLoS One*.  
551 2016;11(3):e0151859.
- 552 18. Fuzzy Analysis (Program FANNY). Finding Groups in Data; 1990:164-198.
- 553 19. Gomes-Silva D, Mukherjee M, Srinivasan M, et al. Tonic 4-1BB Costimulation in  
554 Chimeric Antigen Receptors Impedes T Cell Survival and Is Vector-Dependent. *Cell Rep*.  
555 2017;21(1):17-26.
- 556 20. Frigault MJ, Lee J, Basil MC, et al. Identification of chimeric antigen receptors that  
557 mediate constitutive or inducible proliferation of T cells. *Cancer Immunol Res*.  
558 2015;3(4):356-367.
- 559 21. Long AH, Haso WM, Shern JF, et al. 4-1BB costimulation ameliorates T cell  
560 exhaustion induced by tonic signaling of chimeric antigen receptors. *Nat Med*.  
561 2015;21(6):581-590.
- 562 22. Singh N, Frey NV, Engels B, et al. Antigen-independent activation enhances the  
563 efficacy of 4-1BB-costimulated CD22 CAR T cells. *Nat Med*. 2021;27(5):842-850.
- 564 23. Wang Y, Tong C, Dai H, et al. Low-dose decitabine priming endows CAR T cells  
565 with enhanced and persistent antitumour potential via epigenetic reprogramming. *Nat*  
566 *Commun*. 2021;12(1):409.
- 567 24. Allan SE, Crome SQ, Crellin NK, et al. Activation-induced FOXP3 in human T  
568 effector cells does not suppress proliferation or cytokine production. *Int Immunol*.  
569 2007;19(4):345-354.
- 570 25. Ran Q, Hao P, Xiao Y, et al. CRIF1 interacting with CDK2 regulates bone marrow  
571 microenvironment-induced G0/G1 arrest of leukemia cells. *PLoS One*. 2014;9(2):e85328.
- 572 26. Soroosh P, Ine S, Sugamura K, Ishii N. OX40-OX40 ligand interaction through T  
573 cell-T cell contact contributes to CD4 T cell longevity. *J Immunol*. 2006;176(10):5975-5987.
- 574 27. Holling TM, van der Stoep N, Quinten E, van den Elsen PJ. Activated human T cells  
575 accomplish MHC class II expression through T cell-specific occupation of class II  
576 transactivator promoter III. *J Immunol*. 2002;168(2):763-770.
- 577 28. Gourley TS, Chang CH. Cutting edge: the class II transactivator prevents activation-  
578 induced cell death by inhibiting Fas ligand gene expression. *J Immunol*. 2001;166(5):2917-  
579 2921.
- 580 29. Betts MR, Nason MC, West SM, et al. HIV nonprogressors preferentially maintain  
581 highly functional HIV-specific CD8+ T cells. *Blood*. 2006;107(12):4781-4789.
- 582 30. Caccamo N, Guggino G, Joosten SA, et al. Multifunctional CD4(+) T cells correlate  
583 with active Mycobacterium tuberculosis infection. *Eur J Immunol*. 2010;40(8):2211-2220.
- 584 31. Rossi J, Paczkowski P, Shen YW, et al. Preinfusion polyfunctional anti-CD19  
585 chimeric antigen receptor T cells are associated with clinical outcomes in NHL. *Blood*.  
586 2018;132(8):804-814.
- 587 32. Xhangolli I, Dura B, Lee G, Kim D, Xiao Y, Fan R. Single-cell Analysis of CAR-T  
588 Cell Activation Reveals A Mixed TH1/TH2 Response Independent of Differentiation.  
589 *Genomics Proteomics Bioinformatics*. 2019;17(2):129-139.
- 590 33. Spiegel JY, Patel S, Muffly L, et al. CAR T cells with dual targeting of CD19 and  
591 CD22 in adult patients with recurrent or refractory B cell malignancies: a phase 1 trial. *Nat*  
592 *Med*. 2021;27(8):1419-1431.
- 593 34. Van Gassen S, Callebaut B, Van Helden MJ, et al. FlowSOM: Using self-organizing  
594 maps for visualization and interpretation of cytometry data. *Cytometry A*. 2015;87(7):636-  
595 645.
- 596 35. Rachmilewitz J, Lanzavecchia A. A temporal and spatial summation model for T-cell  
597 activation: signal integration and antigen decoding. *Trends Immunol*. 2002;23(12):592-595.

- 598 36. Weng NP, Araki Y, Subedi K. The molecular basis of the memory T cell response:  
599 differential gene expression and its epigenetic regulation. *Nat Rev Immunol*. 2012;12(4):306-  
600 315.
- 601 37. Sun C, Shou P, Du H, et al. THEMIS-SHP1 Recruitment by 4-1BB Tunes LCK-  
602 Mediated Priming of Chimeric Antigen Receptor-Redirected T Cells. *Cancer Cell*.  
603 2020;37(2):216-225 e216.
- 604 38. Sheih A, Voillet V, Hanafi LA, et al. Clonal kinetics and single-cell transcriptional  
605 profiling of CAR-T cells in patients undergoing CD19 CAR-T immunotherapy. *Nat*  
606 *Commun*. 2020;11(1):219.
- 607 39. Castellino F, Huang AY, Altan-Bonnet G, Stoll S, Scheinecker C, Germain RN.  
608 Chemokines enhance immunity by guiding naive CD8+ T cells to sites of CD4+ T cell-  
609 dendritic cell interaction. *Nature*. 2006;440(7086):890-895.
- 610 40. Bai Z, Lundh S, Kim D, et al. Single-cell multiomics dissection of basal and antigen-  
611 specific activation states of CD19-targeted CAR T cells. *J Immunother Cancer*. 2021;9(5).

613

## 614 **Figure legends**

### 615 **Figure 1: Generation and phenotypic characterisation of CAR T-cells from HD-PBMCs.**

616 **A** Experimental workflow. Peripheral Blood Mononuclear Cells (PBMCs) were isolated from HDs and  
617 LV transduced to express CD19 CAR construct (FMC63 or CAT) following overnight activation with  
618 CD3/CD28 beads. Six days after transduction, CAR T-cells were cultured without (unstimulated) or  
619 with target cells (NALM6) at 1:1 ratio (stimulated). Unstimulated and stimulated cells were analysed  
620 by flow cytometry and sorted for RNA-sequencing 24 hours post-stimulation. Mass cytometry  
621 analysis was performed on unstimulated and stimulated cells at 24 h post-stimulation. Activated  
622 UNTR T-cells were used as a control throughout the experiment.

623 **B** (left) Spaghetti plots showing transduction levels of CAR T-cells as percentage of mCherry+ (in  
624 CD3+) and (right) as MFI of mCherry in unstimulated transduced T-cells measured by FACS 7 days  
625 post-transduction. Lines connect results from individual donors (n= 12 HDs, n = 3 independent  
626 experiments).

627 **C** Spaghetti plot showing the percentage of surface CAR expression (in CD3+) in unstimulated  
628 transduced T-cells measured by FACS 10 days post-transduction. Lines connect results from  
629 individual donors (n = 4 HDs, n = 1 independent experiment).

630 **D** Variation (log<sub>2</sub> fold change) of CD4 and CD8 proportion in unstimulated UNTR T-cells and FMC63  
631 and CAT CAR T-cells measured by FACS 7 days post-transduction. The dotted horizontal line (0)  
632 represents the conditions in which CD4=CD8. Data represent mean ± se (n = 12 HDs, n = 3  
633 independent experiments).

634 **E** (left) Barplots showing the percentage of TCM (CD45RA-CD62L+), (middle) TEM (CD45RA-CD62L-)  
635 and (right) TEMRA (CD45RA+CD62L-) in unstimulated CD3+ UNTR T-cells and FMC63 and CAT CAR T-  
636 cells measured by FACS 10 days post-transduction. Data represent mean ± se (n = 7 HDs, n = 2  
637 independent experiments).

638 **B-E** Statistical significance was calculated by Paired t-test. \*P < 0.05, \*\*P < 0.01, \*\*\*\*P < 0.0001.

639 Each experimental condition is indicated by a specific colour code (UNTR light grey, FMC63 light  
640 blue, CAT orange).

641

642 **Figure 2: RNA-seq and mass cytometry analyses of unstimulated untransduced and CAR-**  
643 **transduced T-cells.**

644 **A** PCA of the top 500 variable genes from RNA-seq analysis across all the experimental conditions (n  
645 = 6 HDs, n = 2 independent experiments).

646 **B** PCA of mass cytometry EMD scores computed at 24 h post-stimulation in CD3+ cells across all the  
647 experimental conditions (n = 4 HDs, n = 1 independent experiment).

648 **C** Fuzzy clustering analysis of RNA-seq data across all experimental conditions (n = 6 HDs, n = 2  
649 independent experiments).

650 **D** (top) Volcano plot showing DE genes between unstimulated FMC63 and CAT CAR T-cells. The  
651 dashed horizontal line represents the statistical significance threshold (FDR < 0.1). (bottom) The  
652 barplots show the expression of selected DE genes (FDR < 0.1) in unstimulated untransduced and  
653 transduced T-cells. Data represent mean ± se (n = 6 HDs, n = 2 independent experiments).

654 **E** The barplots show the expression of mass cytometry EMD scores for Granzyme B, Perforin B, HLA-  
655 DR, CD25, NFAT1, pZAP70 and pS6 in unstimulated CAR T-cells at 24 h upon stimulation. The data

656 shown are normalized to stimulated CD3+ UNTR T-cells. The dotted horizontal line (0) represents the  
657 expression of a specific marker in unstimulated CD3+ UNTR T-cells. Data represent mean  $\pm$  se (n = 7  
658 HDs, n = 2 independent experiments). Statistical significance was calculated by Paired t-test. \*P <  
659 0.05, \*\*P < 0.01.

660 **A-E** Each experimental condition is indicated by a specific colour code (Unstimulated conditions =  
661 UNTR light grey, FMC63 light blue, CAT orange; stimulated conditions = UNTR grey, FMC63 blue, CAT  
662 red).

663

664 **Figure 3: Phenotypic and molecular characterisation of stimulated CAR-transduced T-cells.**

665 **A** Variation (log<sub>2</sub> fold change) of CD4 and CD8 proportion in stimulated UNTR T-cells and FMC63 and  
666 CAT CAR T-cells measured by FACS (n = 12 HDs, n = 3 independent experiments). The dotted  
667 horizontal line (0) represents the conditions in which CD4=CD8.

668 **B** Barplot showing the percentage of TCM (CD45RA-CD62L+) in stimulated CD3+ UNTR T-cells and  
669 FMC63 and CAT CAR T-cells measured by FACS 96h post-antigen stimulation (n = 7 HDs, n = 2  
670 independent experiments).

671 **C** Barplots showing the expression of T-cell exhaustion markers (PD1, TIM3 and LAG3) as MFI in  
672 stimulated CD3+ UNTR T-cells and FMC63 and CAT CAR T-cells measured by FACS 96h post-antigen  
673 stimulation (n = 4 HDs, n = 1 independent experiment).

674 **D** (left) Volcano plot showing DE genes between FMC63 and CAT CAR T-cells upon NALM6 co-  
675 culture. The dashed horizontal line represents the statistical significance threshold (FDR < 0.1).  
676 (right) The barplots show the expression of selected DE genes (FDR < 0.1) in stimulated UNTR T-cells  
677 and in CAR T-cells (n = 6 HDs, n = 2 independent experiments).

678 **E** The barplots show the expression of mass cytometry EMD scores for CD25, HLA-DR, NFAT1,  
679 FOXP3, pZAP70, pS6, pp38, pCREB, pRB and CD4 in stimulated CAR T-cells at 24 h upon stimulation.  
680 The data shown are normalized to stimulated CD3+ UNTR T-cells. The dotted horizontal line (0)

681 represents the expression of a specific marker in stimulated CD3+ UNTR T-cells. (n = 7 HDs, n = 2  
682 independent experiments).

683 **A-E** Barplots show mean  $\pm$  se. Each experimental condition is indicated by a specific colour code  
684 (UNTR grey, FMC63 blue, CAT red).

685 **A, B, C, E** Statistical significance was calculated by Paired t-test. \*P < 0.05, \*\*P < 0.01, \*\*\*P < 0.001,  
686 \*\*\*\*P < 0.0001.

687

688 **Figure 4: Cytokine polyfunctionality in stimulated CAR-transduced T-cells.**

689 **A** The barplots show the expression of mass cytometry EMD scores for effector (Granzyme B, IFN- $\gamma$ ,  
690 TNF- $\alpha$ ) and stimulatory (GM-CSF, IL-2) cytokines in stimulated CAR T-cells. The data shown are  
691 normalized to stimulated CD3+ UNTR T-cells. The dotted horizontal line (0) represents the  
692 expression of a specific marker in stimulated CD3+ UNTR T-cells. (n = 7 HDs, n = 2 independent  
693 experiments).

694 **B** Barplots showing the mean cytokine polyfunctionality in stimulated CAR T-cells, normalized to  
695 stimulated CD3+ UNTR T-cells. The dotted horizontal line (1) represents the mean polyfunctionality  
696 in stimulated CD3+ UNTR T-cells. (n = 7 HDs, n = 2 independent experiments).

697 **C** The stacked barplots show the percentage of stimulated CAR T cells (CD3+mCherry+) expressing 1  
698 to 4 or  $\geq$ 5 cytokines/cell as measured by mass cytometry.

699 **D** The circo plots show all the combinations of the 8 cytokines analysed in stimulated FMC63 (left)  
700 and CAT (right) CAR T-cells by mass cytometry. The numbers indicate patterns of cytokine co-  
701 expression (from 1 to 4 or  $\geq$ 5 cytokines/cell). A specific colour code has been assigned to each  
702 cytokine.

703 **A-B** Data represent mean  $\pm$  se. Statistical significance was calculated by Paired t-test. \*P < 0.05, \*\*\*P  
704 < 0.001.

705 Each experimental condition is indicated by a specific colour code (FMC63 blue, CAT red).

706

707 **Figure 5: Molecular characterisation of CAR T-cells generated from CD19-depleted PBMCs.**

708 **A** (left) UMAP representation of the 4 cell populations (CD8, CD4, CD3 low/neg, CD19) identified by

709 FlowSOM analysis in 4 representative unstimulated samples analysed by mass cytometry at 24 h

710 post-stimulation (n = 4 HDs, n = 1 independent experiment). The cell types are indicated by different

711 colours. (right) Percentage of residual B-cells detected by mass cytometry in unstimulated samples

712 at 24 h post-stimulation. (n = 7 HDs, n = 2 independent experiments).

713 **B** (left) Barplots showing the percentage of TCM (CD45RA-CD62L+) and (right) TEM (CD45RA-CD62L-)

714 in unstimulated CD19-depleted CD3+ UNTR T-cells and FMC63 and CAT CAR T-cells measured by

715 FACS (n = 4 HDs, n = 1 independent experiment).

716 **C** The barplots show the expression of mass cytometry EMD scores for Granzyme B, Perforin B, HLA-

717 DR, CD25, NFAT1, pZAP70 and pS6 in unstimulated CD19-depleted CAR T-cells at 24 h upon

718 stimulation. The data shown are normalized to stimulated CD3+ UNTR T-cells. The dotted horizontal

719 line (0) represents the expression of a specific marker in unstimulated CD3+ CD19-depleted UNTR T-

720 cells. (n = 3 HDs, n = 1 independent experiment).

721 **D** The barplots show the expression of mass cytometry EMD scores for CD25, HLA-DR, NFAT1,

722 pZAP70, pS6, pp38, pRB and CD4 in stimulated CD19-depleted CAR T-cells at 24 h upon stimulation.

723 The data shown are normalized to stimulated CD3+ UNTR T-cells. The dotted horizontal line (0)

724 represents the expression of a specific marker in stimulated CD19-depleted CD3+ UNTR T-cells. (n =

725 3 HDs, n = 1 independent experiment).

726 **E** Barplots showing the mean polyfunctionality in CD19-depleted CAR T-cells at 24 h upon

727 stimulation. The data shown are normalized to stimulated CD3+ UNTR T-cells. The dotted horizontal

728 line (1) represents the mean polyfunctionality in stimulated CD3+ CD19-depleted UNTR T-cells. (n = 3

729 HDs, n = 1 independent experiment).

730 **A-E** Each experimental condition is indicated by a specific colour code (Unstimulated conditions =

731 UNTR light grey, FMC63 light blue, CAT orange; stimulated conditions = FMC63 blue, CAT red).

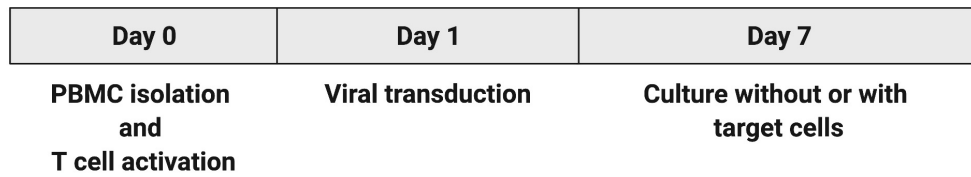
732 Barplots show mean  $\pm$  se. Statistical significance was calculated by Paired t-test. \*P < 0.05, \*\*P <  
733 0.01.

# Figure 1

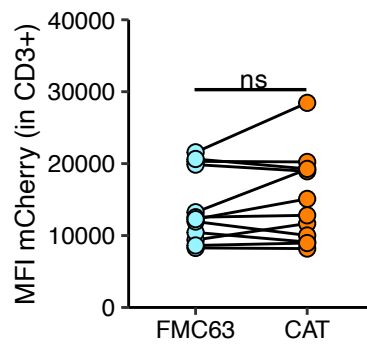
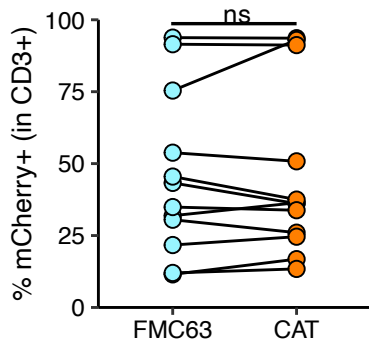
## FIGURE 1

FACS analysis and sorting (1,000 cells) for RNA-sequencing

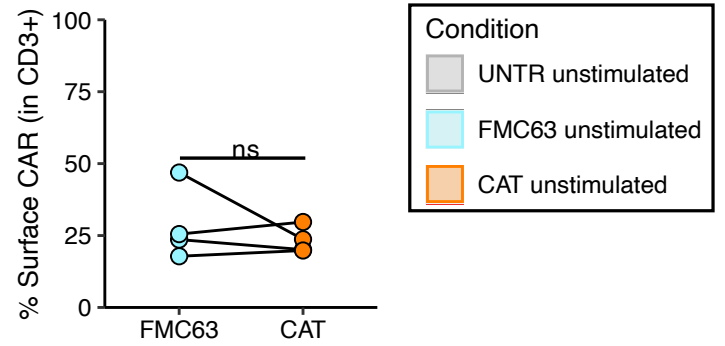
Mass cytometry analysis



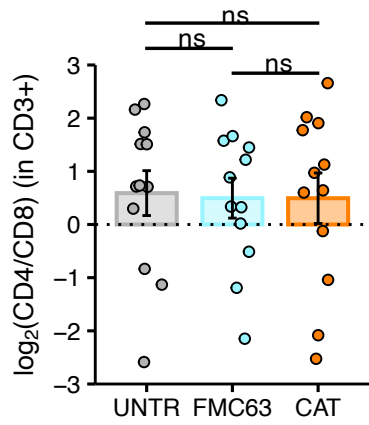
**B**



**C**



**D**



**E**

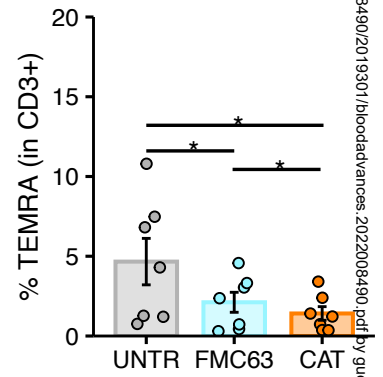
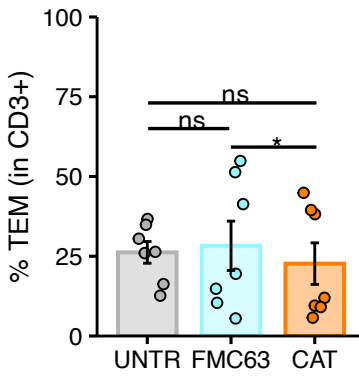
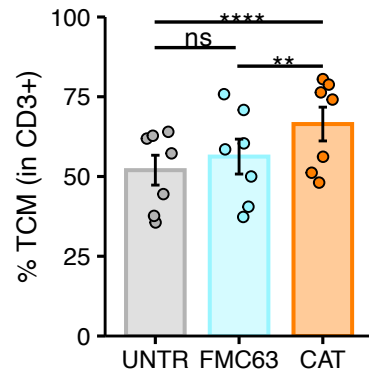
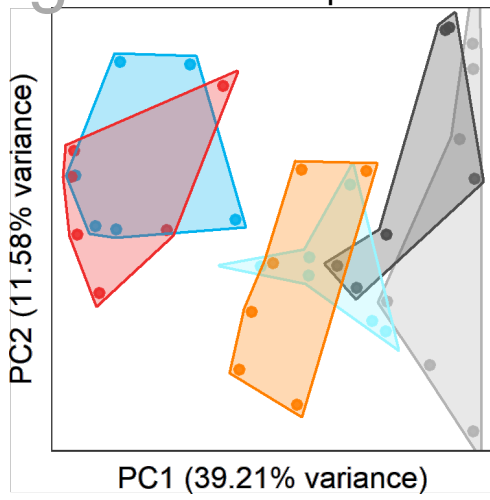
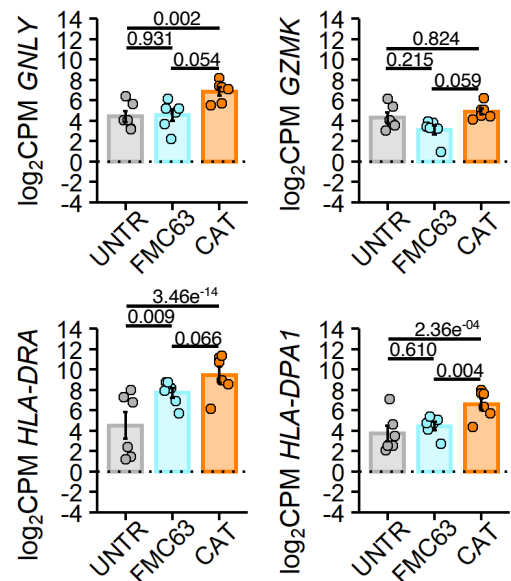
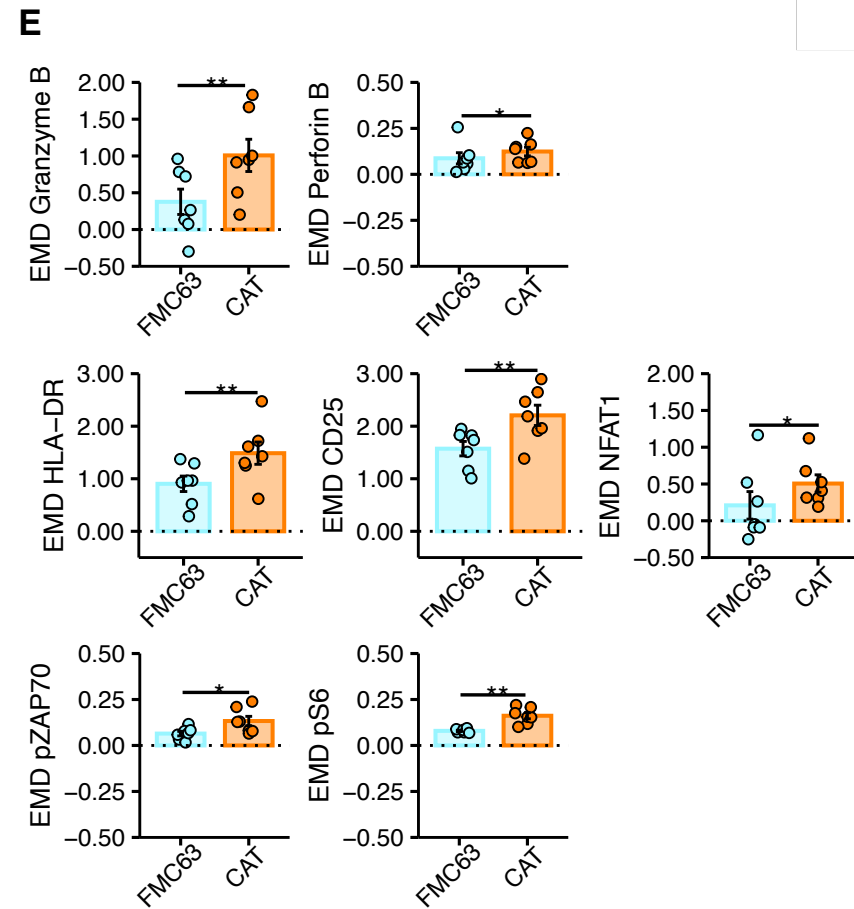
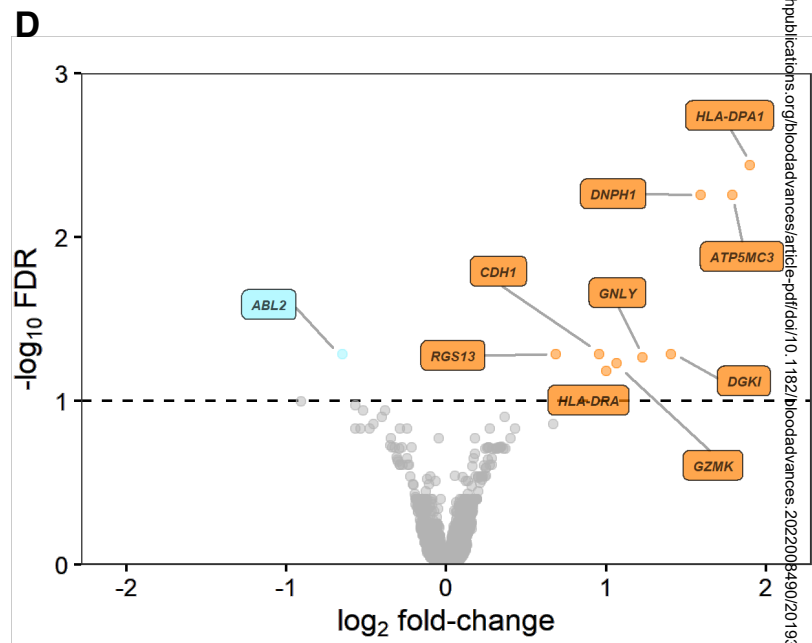
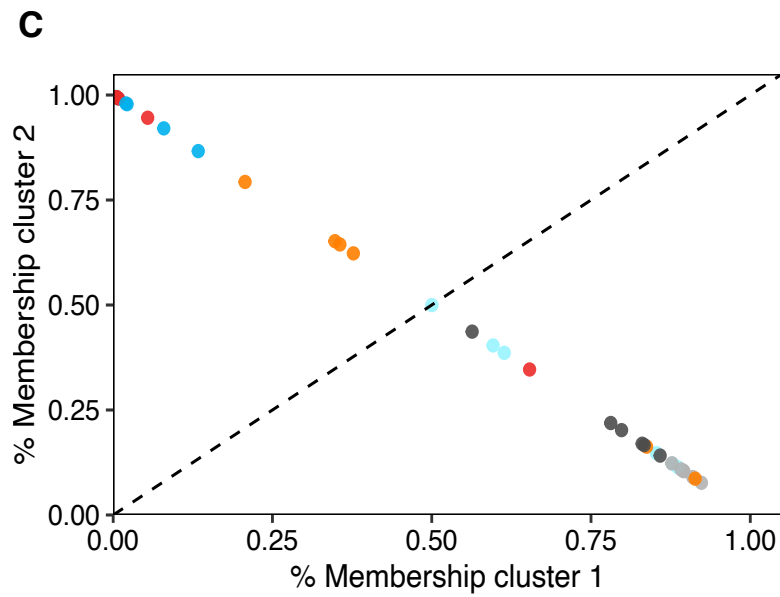
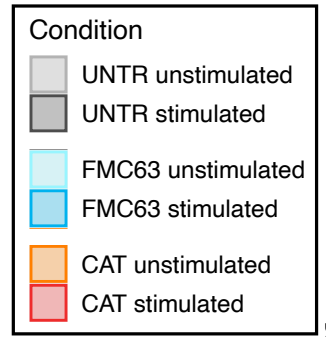
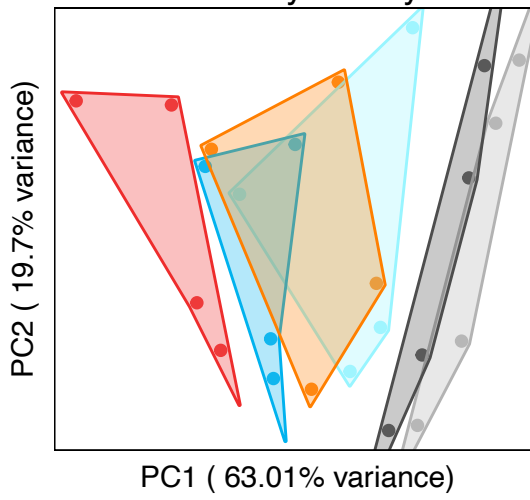




**Figure 2**  
RNA-seq



**B**  
Mass cytometry



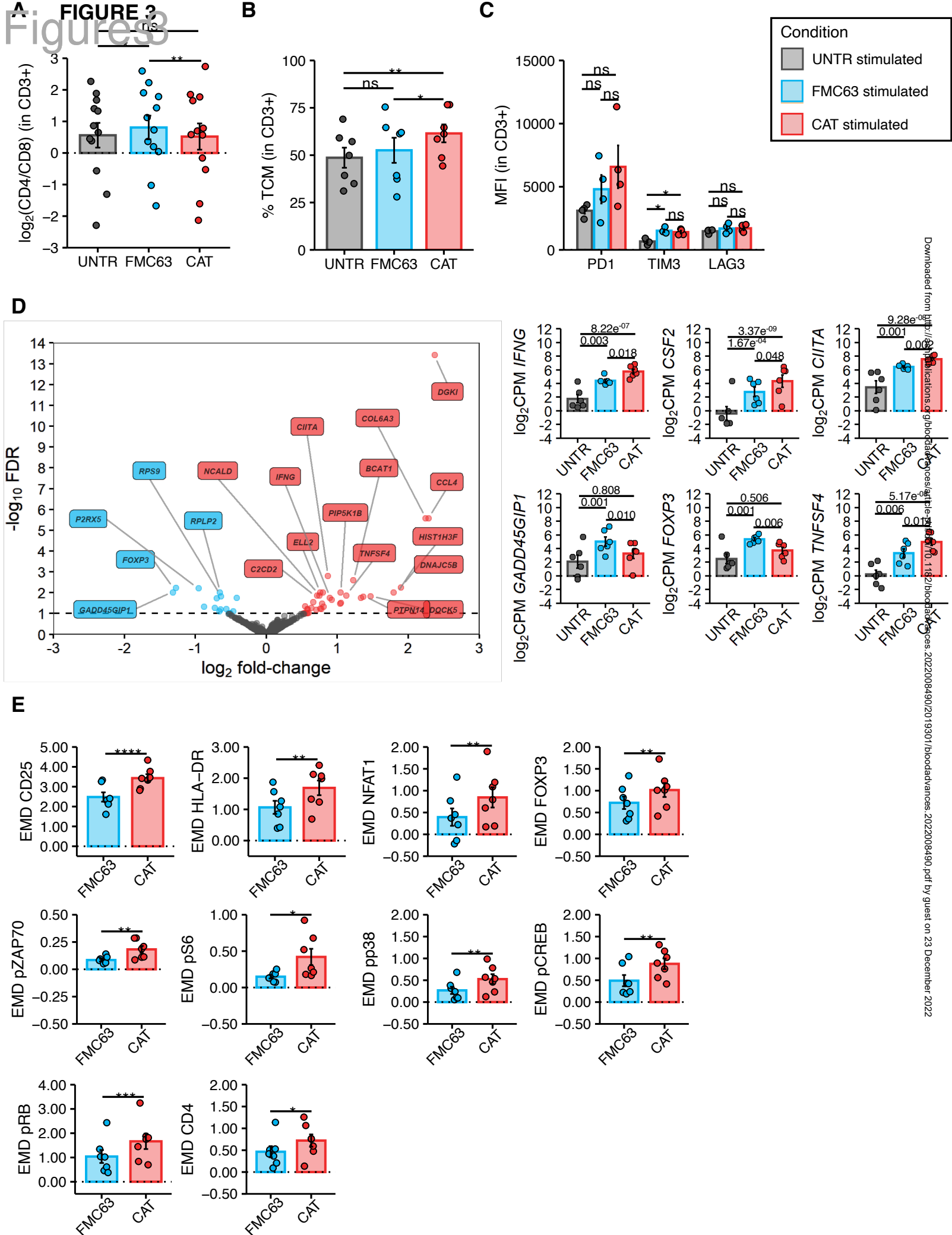
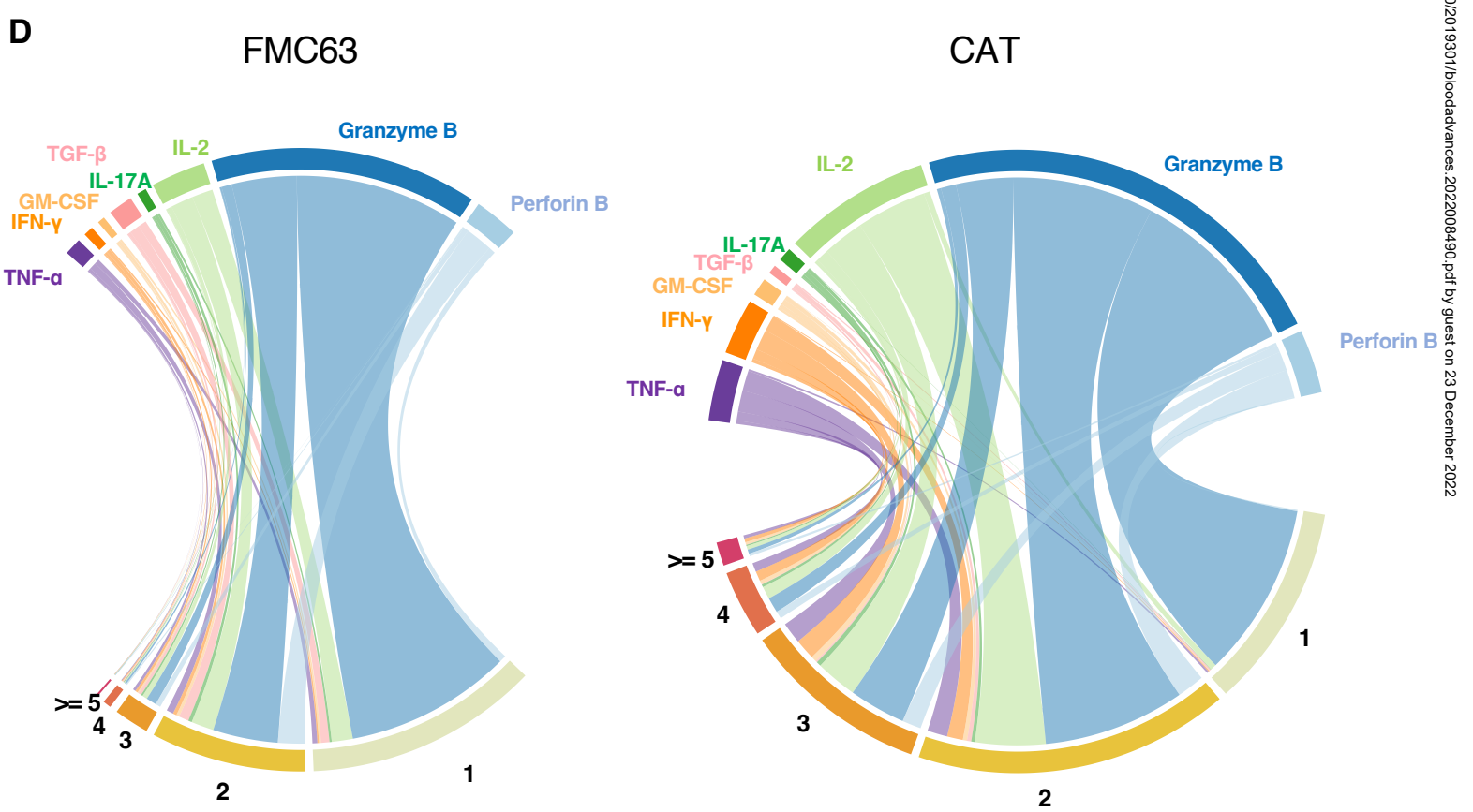
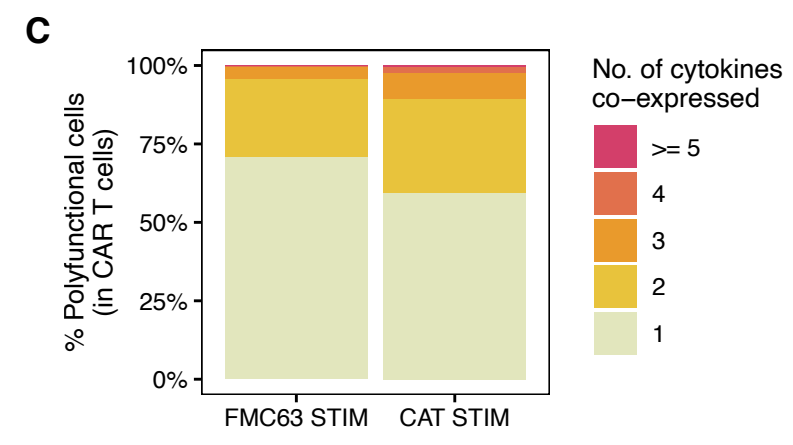
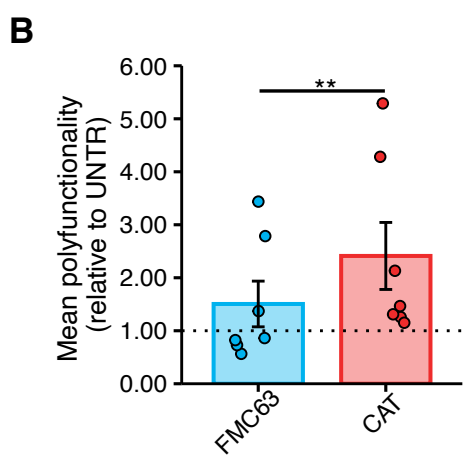
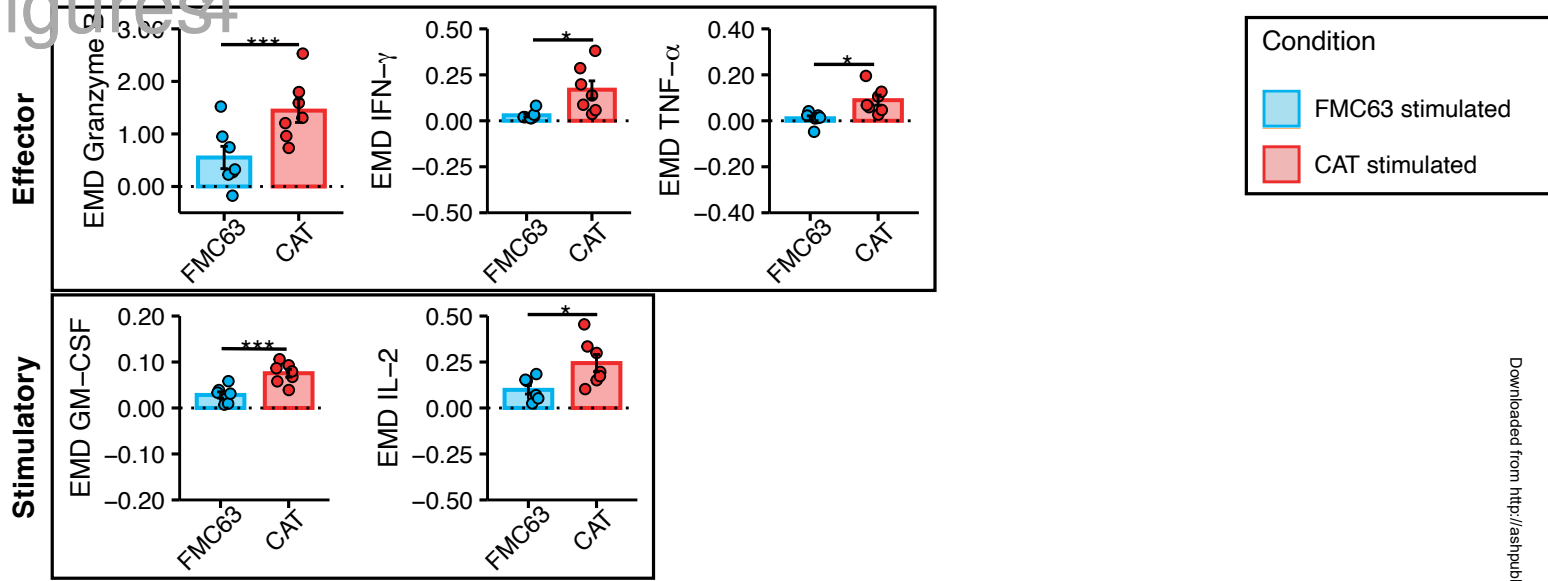
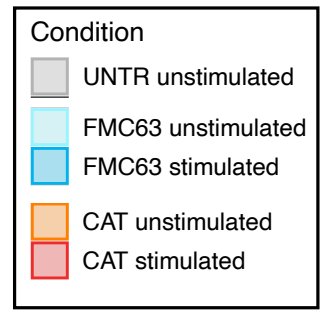
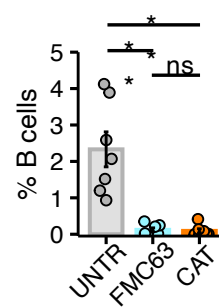
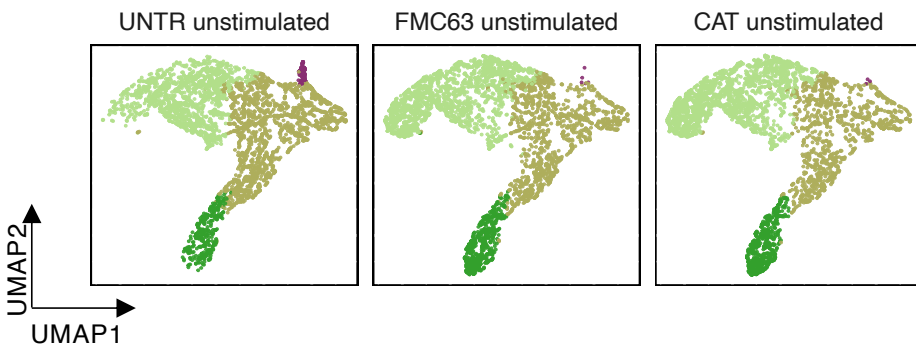


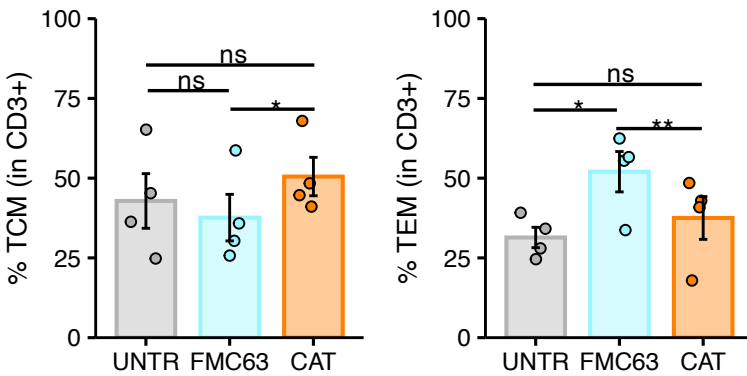
# Figure 4



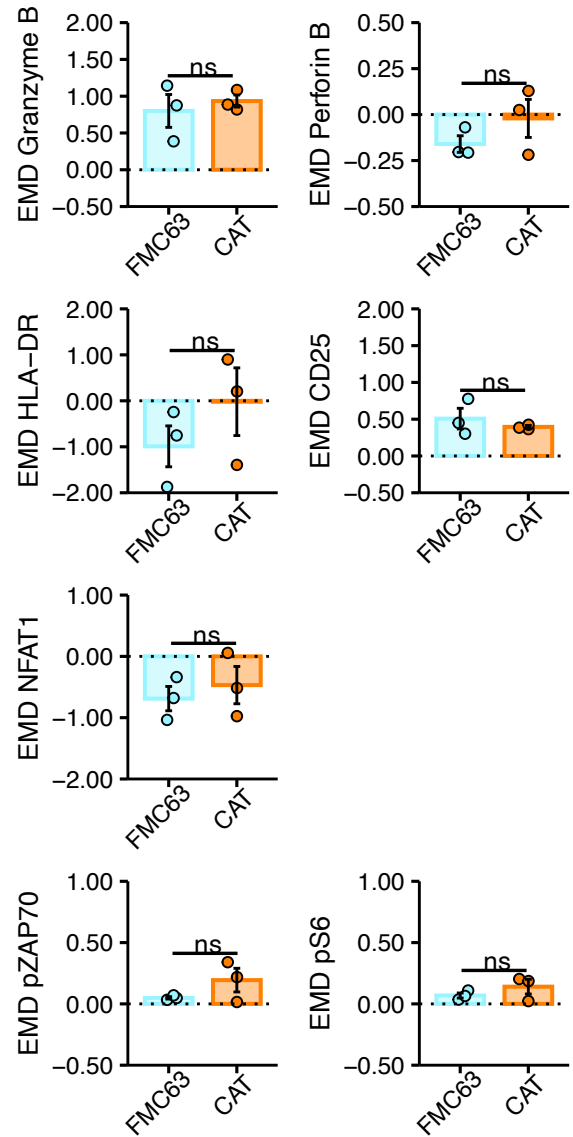
**A** ● CD8 ● CD4 ● CD3 low/neg ● CD19



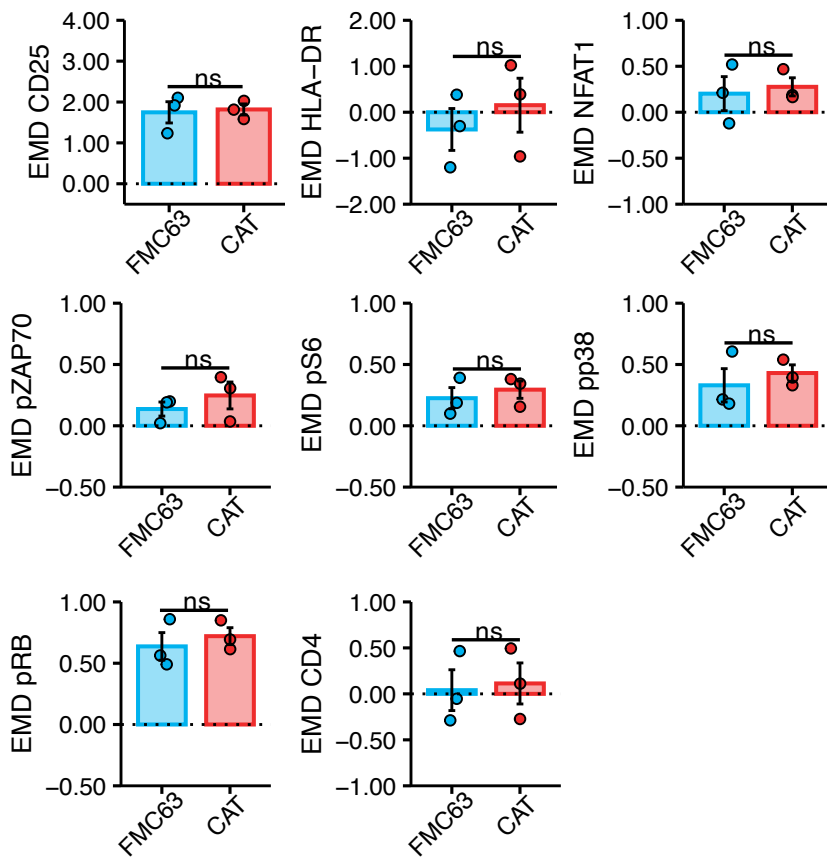
**B**



**C**



**D**



**E**

